ADVANCED FUNCTIONAL MATERIALS
www.afm-journal.de

Low-Temperature Transport in Crystalline $Ge_1Sb_2Te_4$

*Hanno Volker, Peter Jost, and Matthias Wuttig**

Disorder and its reduction upon annealing play a crucial role in understanding the electrical transport in the crystalline phase-change material $Ge_1Sb_2Te_4$. Previous studies focus either on the impact of disorder at moderate temperatures or on the low-temperature properties of crystalline films with a low degree of disorder. The present investigation describes and discusses the impact of pronounced disorder on charge transport at low temperatures. The present data reveal the existence of a metal-to-insulator transition (MIT), where upon increasing order the zero-temperature limit of conductivity changes from zero (insulator) to nonzero values (metal). The position of the MIT is determined with respect to the control parameter, i.e., the disorder, which is modified through the annealing conditions. Disorder is shown to localize carriers for an exceptionally large density of states. In the most disordered films, variable range hopping is observed, enabling the determination of the localization length. At the lowest temperatures studied, deviations from Mott variable range hopping are observed, which can be explained by a transition to Efros–Shklovskii hopping due to the presence of a soft Coulomb gap.

1. Introduction

The pseudo-binary alloys between GeTe and Sb_2Te_3 (GST) belong to the class of phase-change materials (PCMs). These compounds are characterized by a prominent optical and electrical contrast between the amorphous and the crystalline phase and can be rapidly and reversibly switched between these two states. While the reflectivity contrast has been exploited for rewritable optical data storage, the contrast in electrical resistivity opens up the opportunity of building nonvolatile electrical memories with switching times of the order of nanoseconds and below.[1–3]

Most GST compounds possess a stable trigonal crystal structure and a meta-stable, locally distorted rocksalt structure where Te atoms occupy one fcc sublattice and Ge atoms, Sb atoms and vacancies share the other.[4–6] This crystalline phase is obtained upon crystallization at moderate temperatures. It is also the crucial crystalline phase for data storage applications since it is formed by short laser pulses (optical data storage) or short voltage pulses (electronic memories). The properties of crystalline phases of PCMs are governed by their special bonding mechanism, which is characterized by resonating covalent p-bonds.[7] These bonds form due to the low tendency of PCMs to realize either ionic bonds or sp-hybridization.[8]

Many of the GST materials such as $Ge_1Sb_2Te_4$ (GST124) display another prominent feature: Upon crystallization, their electrical resistivity—albeit orders of magnitude below its value in the amorphous phase—starts high and can be decreased tremendously upon annealing.[9,10] This effect is accompanied by a continuous change in the temperature coefficient of resistivity (TCR) which eventually changes its sign from negative to positive. The high resistivity and the negative TCR have been attributed to disorder-induced localization[11] of carriers in the vicinity of vacancy clusters which are due to the random occupation of the Ge/Sb/vacancy lattice sites.[12] These localization effects dominate the electrical transport even at room temperature, as evidenced from a high resistivity, a negative TCR and a small mean-free path. Grain boundaries, on the contrary, do not provide the dominant contribution to scattering, as can also be seen from data on single crystalline GeTe nanowires, which also reveal disorder-induced localization.[13]

Recently, we have investigated[14] the charge transport in metallic films of crystalline phase-change materials, i.e., samples with a low degree of disorder. In these films, disorder-induced electron–electron interaction and weak antilocalization were observed at low temperatures. However, in these samples the disorder was insufficient to create an insulating state at low temperature. Above a certain level of disorder, carriers are expected to be strongly localized and the zero-temperature limit of the conductivity should be zero, which is the commonly accepted criterion for an insulator. Hence, a disorder-driven metal-to-insulator transition takes place. Metal–insulator transitions (MITs) have been observed and thoroughly studied in a variety of material systems, such as doped single-crystalline semiconductors,[15–17] amorphous transition-metal/semiconductor alloys,[18,19] or quasicrystals.[20–22] All these studies rely on low-temperature transport measurements in the vicinity of the MIT. While the high-temperature properties of both weakly and strongly disordered GST124 thin-film samples as well as the low-temperature behavior of weakly disordered films have been studied by Siegrist et al.[11] and Breznay et al.,[14] respectively,

Dr. H. Volker, Dr. P. Jost, Prof. M. Wuttig
Institute of Physics (IA)
RWTH Aachen University
52056 Aachen, Germany
E-mail: wuttig@physik.rwth-aachen.de
Prof. M. Wuttig
Jülich-Aachen Research Alliance
Section Fundamentals of Future Information Technology (JARA-FIT)
52056 Aachen, Germany

DOI: 10.1002/adfm.201500830

Table 1. List of samples investigated and their properties. The different substrates are: sapphire ("sap."), glass and silicon with a thermal oxide of 1 µm thickness ("Si"). Employing shadow masks during the deposition, the films were patterned in Hall-bar ("Hall") or van-der-Pauw ("vdP") geometry. The other parameters listed are: film thickness d, nominal annealing temperature T_{anneal}, room-temperature conductivity σ(300 K), room-temperature Hall carrier concentration n_H(300 K), the conductivity ratio $r\sigma = \sigma/\sigma_{min}$, and the temperature coefficient of resistivity $\mathrm{TCR} = \left.\frac{dR/dT}{R}\right|_{270K}$. The last two columns indicate the metallic or insulating nature of the samples by listing the extrapolated value of α from Equation (6) and the sign of the slope of $w(T)$ as defined in Equation (7) at the lowest accessible temperature (LAT), respectively.

	Subst.	Geom.	d [nm]	T_{anneal} [°C]	σ (300 K) [S cm^{-1}]	n_H(300 K) [10^{20} cm^{-3}]	$r\sigma$(= $k_F\lambda$)	TCR [ppm K^{-1}]	α [S cm^{-1}]	sgn(dw/dT) at LAT
A	sap.	Hall	59	175	2.9	1.1	0.007	−10537		
F	sap.	Hall	59	180	4.2	1.4	0.011	−8990		
f	glass	vdP	70	175	6.6	0.9	0.017	−6961		−
g	glass	vdP	70	200	25	1.4	0.064	−3418	−1.1	−
h	glass	vdP	70	225	54	1.5	0.137	−2375	11.2	+
i	glass	vdP	70	250	234	1.9	0.60	−750	167.5	+
j	Si	vdP	70	275	427	2.1	1.09	6		+
e	glass	vdP	70	300	557	2.3	1.42	457		+

the low-temperature transport in strongly disordered samples (i.e., close to the transition and on the insulating side) has not been studied in sufficient detail.

It is the aim of this paper to start filling this gap by investigating the MIT and the transport mechanism in the most disordered samples. Although the temperature-dependence of the resistance of the least ordered sample studied by Siegrist et al.[11] strongly suggests that a MIT takes place, its very existence remains to be verified by measuring the resistivity at temperatures as low as possible and analyzing the data, in particular extrapolating it with commonly accepted methods.

This paper is organized as follows: The preparation of the samples is described in Section 2. In Section 3, details on the electrical measurements are given. In addition, important transport parameters are calculated. Section 4 focuses on the metal-insulator transition, addressing the question whether a MIT exists and, if so, localizing its position in the control parameter space by means of sub-Kelvin measurements and extrapolations to 0 K. Section 5 deals with the low-temperature transport in the most disordered samples. The results are summarized in Section 6.

2. Sample Preparation

Prior to the deposition of the GST material, metallic (Cr + Au) contacts for Hall-bar and van-der-Pauw sample geometries were deposited on cleaned substrates (size: 10 mm × 10 mm) by thermal evaporation through metallic shadow masks. Next, thin films of $Ge_1Sb_2Te_4$ were deposited by DC magnetron sputtering (also through corresponding shadow masks) from stoichiometric targets. The background pressure was always smaller than 2×10^{-6} mbar and the process pressure was of the order of 5×10^{-3} mbar using argon as sputter gas. To protect the film from atmospheric influences, protective layers of at least 20 nm ZnS:SiO_2 (80:20) were deposited on top by RF sputtering before venting the chamber. The thicknesses of the two layers were controlled via the deposition time and afterward precisely measured by means of X-ray reflectometry (XRR). After the deposition of the amorphous films, thermal annealing has been performed at various temperatures in a glass tube with a heating ramp of 5 K min^{-1} and a holding time of 30 min under a continuous flow (200 sccm) of argon. From X-ray diffraction measurements we know that this procedure yields samples that are fully crystalline. **Table 1** provides a list of all samples.

3. Electrical Characterization

Electrical transport measurements were performed in a Quantum Design Physical Property Measurement System (PPMS) in a temperature range between 300 and 2 K. Some of the measurements were extended to 0.35 K employing a PPMS Helium-3 refrigerator. Four-terminal resistance measurements according to the van-der-Pauw method[23] were carried out with the PPMS-internal resistance measurement system ("User Bridge") sourcing a square-wave current and measuring the voltage. The highly resistive Hall-bar samples A and F were measured in a two-terminal geometry employing Quantum Design's Electrical Transport Option (ETO) sourcing a sine voltage and measuring the current. Care was taken to ensure that all measurements were performed in the Ohmic region and the resistance reading was not distorted by the sample's capacitance.

The difference between the various samples that is relevant to electronic transport properties is the annealing state. Hence, the nominal set point T_{anneal} of the furnace seems like a natural choice for labeling the samples. Comparing samples A, F, and f however reveals that differences in the room-temperature conductivity $\sigma_{300\ K}$ are discernible which are beyond the reproducibility of the annealing procedure, probably due to different thermal properties of the substrate and/or variation in sample position within the furnace. $\sigma_{300\ K}$ is much more suitable to characterize the annealing state. As will be seen in the following, all other transport properties, such as the conductivity at any other temperature, the TCR or the localization length

depend systematically on $\sigma_{300\,K}$. Because of its predictive power, and since it is especially simple to measure, we will use $\sigma_{300\,K}$ to refer to a specific sample in the following.

In addition to measurements of the longitudinal resistance in zero field, Hall effect measurements were performed at room temperature in a field range of ±1 T. In this range the transversal resistance R_{xy} is linear in magnetic field. The Hall carrier concentration obtained at 300 K is provided in Table 1. Since upon the metal-insulator transition verified below, the states at the Fermi energy change from localized to delocalized, it is remarkable that the Hall carrier concentration measured at 300 K is only weakly affected by annealing. This observation, already reported by Siegrist et al.,[11] is quite surprising, since the Hall effect is not expected to yield the correct number of carriers once they are localized. However, at 300 K the localization effects are presumably weak enough to recover the correct carrier density in the Hall effect. Hence, we assume that the slight variation in n_H upon annealing is an artifact from residual localization and use the values of n_H obtained on the most metallic sample as a best estimate to calculate the Fermi wave vector

$$k_F = \left(3\pi^2 \frac{n_H}{M}\right)^{1/3} = 1.2\ \mathrm{nm}^{-1} \tag{1}$$

where M denotes the valley degeneracy of[11] $M = 4$, the Fermi energy

$$E_F = \frac{(\hbar k_F)^2}{2m^*} = 0.14\ \mathrm{eV} \tag{2}$$

where m^* denotes the effective mass of[11] $m^* = 0.4m_e$, the density of states at the Fermi energy

$$N(E_F) = \frac{3}{2}\frac{n_H}{E_F} = 2.5\times10^{21}\,\mathrm{cm}^{-3}\,\mathrm{eV}^{-1} \tag{3}$$

and the "minimum metallic conductivity"

$$\sigma_{min} = \left(\frac{M}{3\pi^2}\right)^{2/3} \cdot \frac{e^2}{\hbar} \cdot n_H^{1/3} = 393\ \mathrm{Scm}^{-1} \tag{4}$$

From the latter, we can calculate the resistivity ratio $r_\sigma = \sigma/\sigma_{min}$ for each sample. These numbers are given in Table 1.

We chose the parabolic-band model because of its simplicity and its concomitant unambiguity. The only free parameter is the effective mass. With 2×10^{20} cm^{-3} holes in the valence band, the value of E_F obtained from this model is reasonable, as the 10^{23} cm^{-3} p-electrons form a band which is approximately 6 eV wide.[24] However, in the presence of a high degree of disorder and close to the band edge, the density of states will no longer follow the $\sqrt{E}$ behavior predicted from the parabolic-band model. Instead, exponential tails will appear. Even in amorphous phase-change materials, the characteristic energy γ of the tail is only of the order of 30 meV,[25] which is much smaller than the Fermi energy calculated above. Nevertheless, it is worthwhile to investigate to what extent the numbers above will change if a model with tail states is employed. Hence we consider the "OJL"-model developed by O'Leary et al.[26] In this model, the valence band density of states is given by

$$D(E) = M\frac{(2m^*)^{3/2}}{2\pi^2\hbar^3} \times \begin{cases} \sqrt{-E} & ,\left(E < -\frac{\gamma}{2}\right) \\ \sqrt{\frac{\gamma}{2}} \cdot \exp\left(-\frac{1}{2}\right) \cdot \exp\left(-\frac{E}{\gamma}\right) & ,\left(E \geq -\frac{\gamma}{2}\right) \end{cases} \tag{5}$$

Only one additional parameter γ is introduced compared to the parabolic-band model. When this parameter is varied between 0 and 60 meV, the values of E_F and $N(E_F)$ are only slightly affected and decrease—by only 29% and 12%—to 0.10 eV and 2.2×10^{21} cm^{-3} eV^{-1}, respectively. Therefore, we can stick to the numbers calculated within the parabolic-band model.

4. Metal–Insulator Transition

Figure 1 (top) depicts the resistance as a function of temperature for the 70-nm thick samples. From this figure and from Table 1, the huge variance in room temperature conductivity of about two orders of magnitude can readily be seen. This variation is solely achieved by varying the annealing temperature. Moreover, this spread extends rapidly if the conductivity is measured far below room temperature. In Table 1, this is reflected by the large variation of TCR values. These findings are in line with those reported by Siegrist et al.[11]

As can be seen in Figure 1 (bottom), the high-temperature TCR changes its sign between the samples with room-temperature conductivity values of 234 S cm^{-1} (sample i) and 557 S cm^{-1} (sample e), i.e., around an annealing temperature of 275 °C. Already reported by Siegrist et al.[11], we have connected this TCR sign change to the Ioffe-Regel criterion. In one of its weaker formulations, this criterion asserts that the concept of Bloch states is safely applicable only if the product of the Fermi wave vector k_F and the elastic mean-free path λ exceeds unity. In Equation (4), σ_{min} is constructed in such a way that the conductivity ratio $r\sigma$ is equal to $k_F \times \lambda$ provided that the free carrier model is applicable. The Ioffe-Regel criterion is able to describe some phenomena at elevated temperatures, such as resistivity saturation, if correlation effects are weak.[27] In the case of $Ge_1Sb_2Te_4$, a material with a low degree of correlation,[11] it nicely describes the position of the TCR sign change: Sample i ($\sigma_{300\,K}$ = 234 S cm^{-1}) with a resistivity ratio of $r\sigma \approx 0.6$ displays a negative TCR throughout the entire temperature range, sample j ($\sigma_{300\,K}$ = 427 S cm^{-1}) with a resistivity ratio close to one ($r_\sigma \approx 1.1$) has a very weak and non-monotonic temperature dependence. Sample e ($\sigma_{300\,K}$ = 557 S cm^{-1}) with a resistivity ratio of $r_\sigma \approx 1.4$ displays a positive TCR all the way down to 25 K. Privitera et al. have reported a similar change in the TCR of films of the related compound $Ge_2Sb_2Te_5$ and proposed their application as temperature-independent resistors.[28]

Up to here, we have dealt with the transport at moderate temperatures. By contrast, the distinction of a metal from an

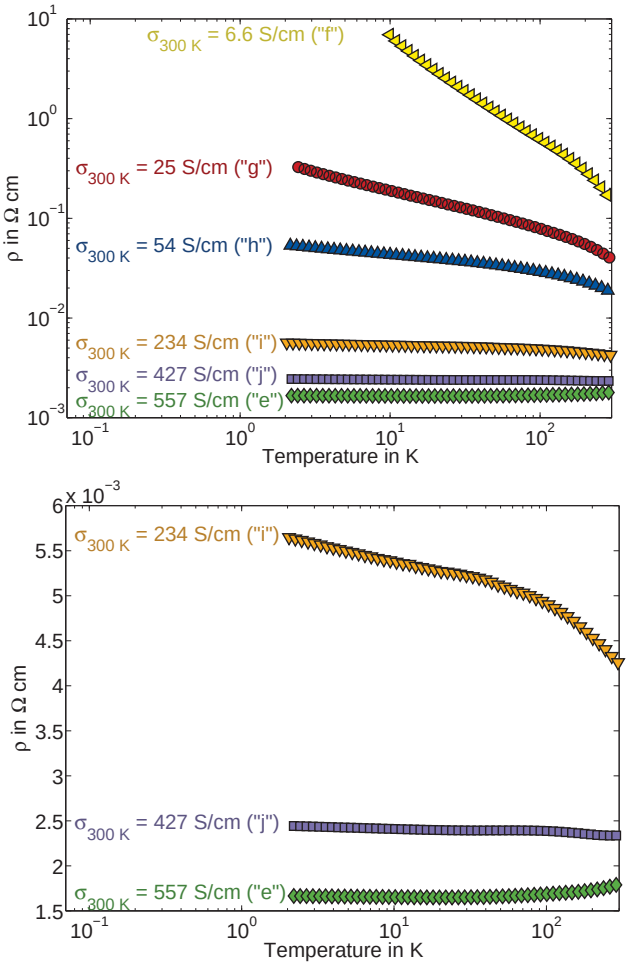

Figure 1. Top: Temperature dependence of the resistivity of 70 nm thick films of $Ge_1Sb_2Te_4$ annealed at different temperatures, which lead to different room-temperature conductivities, used to identify the samples. Bottom: Close-up view of the samples in the vicinity of the TCR sign change.

insulator is given by the non-zeroness of the conductivity in its zero-temperature limit. The application of the ideas behind the Ioffe-Regel criterion led Mott to the proposition of a minimum metallic conductivity,[29] i.e., the smallest possible nonzero value that the conductivity at zero temperature may attain. This is exactly the quantity σ_{min} from Equation (4). Despite the successes of the Ioffe-Regel criterion in describing high-temperature phenomena, the concept of a minimum metallic conductivity has widely been regarded as outdated since the continuous transition described by scaling theory[30] has been confirmed.[15] Also in our case, a sample with negative TCR may well retain a finite resistivity down to 0 K. Hence, the ability of the Ioffe-Regel criterion to describe the TCR sign change observed at elevated temperatures does not imply that the system displays a minimum metallic conductivity in the zero-temperature limit. Therefore, we will now turn our attention toward the conductivity at the lowest temperatures measured and the question whether it remains finite at 0 K.

In order to classify the samples into metallic or insulating, resistance measurements at temperatures down to 0.35 K were

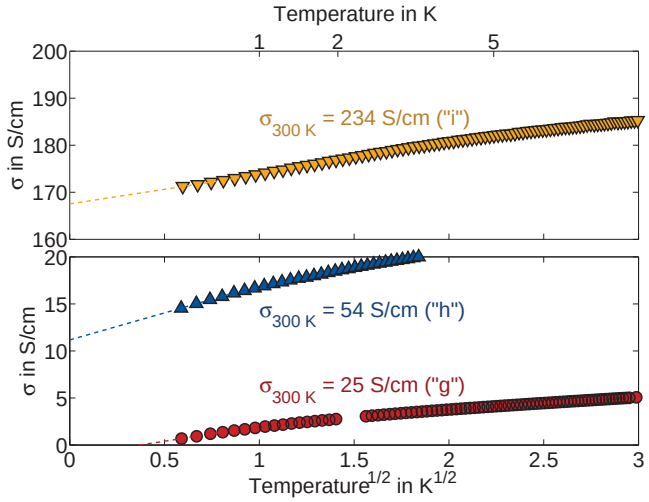

Figure 2. Conductivity plotted against the square root of temperature in order to extrapolate its 0 K limit. Only data obtained on the samples in the vicinity of the MIT are shown. The dashed lines are the suggested extrapolations.

performed on samples with room-temperature conductivity values between 25 and 234 S cm^{-1} (samples g, h, and i). The most widely accepted extrapolation method in order to obtain the zero-temperature limit is to use a functional dependence of the form[31–34]

$$\sigma(T) = \alpha + \beta T^{\nu} \tag{6}$$

with $\beta > 0$ and usually $\nu = 1/2$. For metallic samples, $\sigma(0) = \alpha > 0$, whereas $\alpha = 0$ would imply that the sample is just at the edge of a (continuous) MIT. By contrast, insulating samples are expected to deviate from this law at lowest temperatures (strong localization) but obey it at intermediate temperature, though with $\alpha < 0$.

Figure 2 reveals that the sample with $\sigma_{300\ K}$ = 25 S cm^{-1} (sample g) has a negative α as determined from the lowest-temperature part of the data. By contrast, positive y-intercepts are obtained for the samples with $\sigma_{300\ K}$ = 54 S cm^{-1} and $\sigma_{300\ K}$ = 234 S cm^{-1} (h and i, respectively). This finding corroborates the existence of a metal-to-insulator transition. The y-intercepts α are listed in the second-to-last column of Table 1.

Nevertheless, one can also see that a fit with a $\sqrt{T}$ behavior only describes a limited temperature range. This also holds if the data are plotted with $\sqrt[3]{T}$ as the abscissa (not shown), raising doubt about the reliability of this kind of extrapolation. Hence, we have also tried to locate the MIT by using the logarithmic derivative[35,36]

$$w(T) = \frac{\mathrm{d}\ln\sigma}{\mathrm{d}\ln T} \tag{7}$$

This method does not reduce the requirements in terms of low-temperature data. If in the low-temperature limit this quantity is positive and its slope $\frac{\mathrm{d}w(T)}{\mathrm{d}T}$ is negative, the corresponding sample must be insulating. If an insulating sample obeys an Arrhenius- or variable-range hopping law, $w(T)$ should

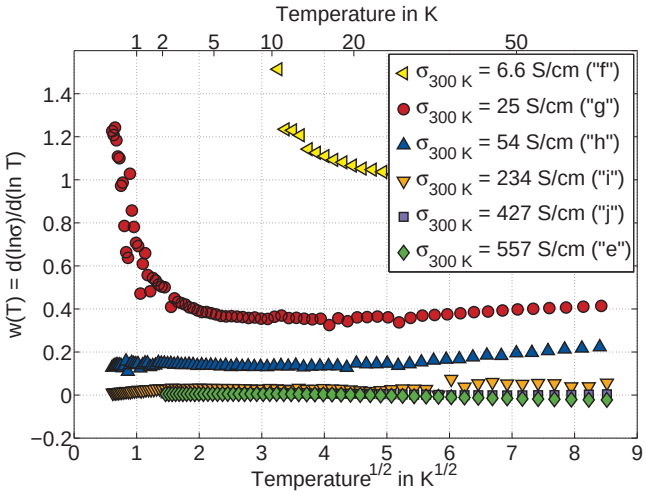

Figure 3. The logarithmic derivative $w(T)$ qualifies the samples with $\sigma_{300\ K} \leq 25$ S cm^{-1} (f and g) clearly as insulating (negative slope in $w(T)$) and samples with $\sigma_{300\ K} \geq 234$ S cm^{-1} (i, j, and e) as metallic. The $w(T)$ for the sample with $\sigma_{300\ K} = 54$ S cm^{-1} (h) displays a subtle, but discernible positive slope at lowest measurement temperatures. It is thus deemed to be metallic rather than insulating.

diverge for $T \to 0$. For metallic samples fulfilling Equation (6), $w(T)$ tends to zero for $T \to 0$ and in case of a just-critical sample, $w(T)$ is expected to approach a constant value.

The advantage of this method is that it is considered to be less biased, as compared to the assumption of a specific law such as Equation (6). The calculation of $w(T)$ requires data of high density and low noise. Also, measurements for such an analysis should extend to very low temperatures, be performed at a well-controlled and sufficiently small temperature ramp and in the dark to exclude any effects of photoconductivity superimposed with the temperature-dependence of resistance. These requirements are fulfilled for the present data set. The logarithmic derivative is obtained from the data by partwise-fitting of a linear function to $\ln\sigma$ versus $\ln T$ and is displayed in **Figure 3**. Also, the sign of the slope of $w(T)$ is listed in the last column of Table 1. Classifying all samples with room-temperature conductivity values of 25 S cm^{-1} and below as insulating and all samples with room-temperature conductivity values of 54 S cm^{-1} and above as metallic is consistent with both criteria, the $\sqrt{T}$ -extrapolation and the logarithmic derivative.

Hence, we conclude that a MIT is observed, but that its precise position differs from that of the TCR sign change. While the latter takes place very close to $r_\sigma \approx 1$, the former occurs between $r_\sigma \approx 0.06$ and $r_\sigma \approx 0.14$. The smallest metallic zero-temperature conductivity of the present sample series is 11 S cm^{-1}. As this value is far below the calculated minimum metallic conductivity, this implies that in the $T \to 0$ limit we observe a continuous MIT.

5. Transport Properties Far on the Insulating Side

We now turn our attention to the rather insulating samples. As the electronic states around the Fermi energy are localized, the low-temperature electrical transport is expected to be dominated by variable-range hopping. Mott's law for hopping in three dimensions assuming a constant density of states $N(E)$ $N(E_F)$ around the Fermi energy predicts[37]

$$\sigma = \sigma_{0,M} \exp\left[-\left(\frac{T_M}{T}\right)^{1/4}\right] \tag{8}$$

with[38]

$$k_B T_M = \frac{18}{\xi^3 N(E_F)} \tag{9}$$

where ξ is the localization length.

It should be emphasized that a disorder-induced metal–insulator transition with a Fermi energy lying 0.14 eV deep within the valence band is exceptional, especially for a crystalline material. As a consequence, also the density of localized states of $N(E_F) = 2.5 \times 10^{21}$ cm^{-3} eV^{-1} at the Fermi energy is unusually large. Of course much higher carrier densities are present in amorphous metals. However, in amorphous metals carriers are still delocalized and hence no hopping transport can be observed. Instead, some typical values in other systems where variable-range hopping is observed are of the order of $(0.8\ldots3.9) \times 10^{18}$ cm^{-3} eV^{-1} in amorphous IV-semiconductors,[39,40] $(0.8\ldots3.5) \times 10^{20}$ cm^{-3} eV^{-1} in doped crystalline semiconductors,[41,42] or 1.6×10^{20} cm^{-3} eV^{-1} in amorphous indium oxide.[43,44] In crystalline GST124, we have a roughly 10-times higher carrier concentration.

The fact that we observe strong localization despite the huge density of states at the Fermi level points to the exceptionally strong impact of disorder-induced localization effects in GST124. A high level of structural disorder originates from the random distribution of the 25% vacancies on the cation sublattice. In addition, the sensitivity of the electronic states in GST to structural disorder and hence their ability of being easily localized can be attributed to the fact that the valence band is formed by electrons in highly directional p orbitals. By contrast, Hosono suggests that amorphous transparent conductive oxides require the relevant conduction band to be composed of spherical s-electrons in order to be metallic.[45]

In **Figure 4** the resistivity values of the Hall-bar samples with $\sigma_{300\ K} = 2.9$ and $\sigma_{300\ K} = 4.2$ S cm^{-1} (samples A and F, respectively) are plotted on a semilogarithmic scale as a function of $T^{1/4}$. Although the lowest accessible temperature is 0.35 K, the highest resistance that can be reliably measured with the electronics employed is considered to be 10 GΩ, hence the data are cut off at this point. A two-terminal measurement has also been performed on the slightly more conductive sample with $\sigma_{300\ K} = 6.6$ S cm^{-1} (sample f) through its finite-size van-der-Pauw contacts. The effective geometric factor has been obtained from a comparison with the previous van-der-Pauw measurement.

For the sample with $\sigma_{300\ K} = 4.2$ S cm^{-1} (sample F) the curvature of the data is concave at temperatures above 20 K, while it becomes convex below 5 K. Hence Equation (8) is not fulfilled over the whole temperature range displayed in Figure 4. Nevertheless, the region with almost vanishing curvature is quite broad. Also, deviations at higher temperatures are to be expected as other mechanisms such as phonon-induced delocalization and excitation of carriers into delocalized states will start to contribute.

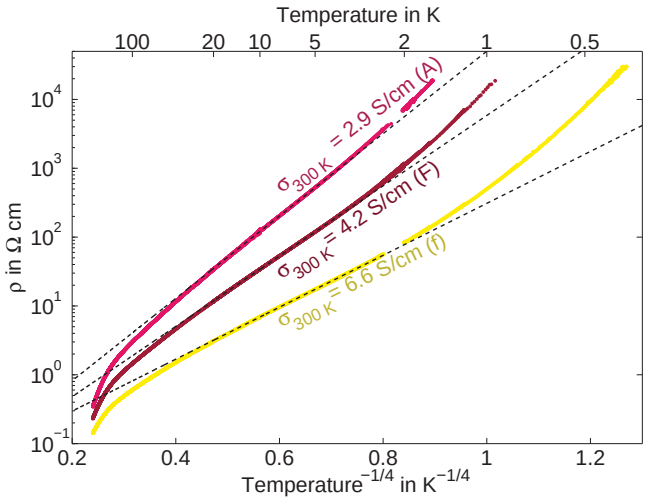

Figure 4. Temperature dependence of the resistance of samples A ($\sigma_{300\,K} = 2.9$ S cm^{-1}), F ($\sigma_{300\,K} = 4.2$ S cm^{-1}), and f ($\sigma_{300\,K} = 6.6$ S cm^{-1}) on a Mott variable range hopping scale. The dashed lines represent the fits of the data between 5 and 20 K to Equation (8) according to the parameters given in Table 2. Details about the sample properties are given in Table 1.

The linear fit performed in the range 5 K $\leq T \leq$ 20 K yields a Mott temperature of 19102 K for this sample. With Equation (9) and $N(E_F) = 2.5 \times 10^{21}$ cm^{-3} eV^{-1}, we thus obtain a localization length of 1.6 nm.

According to the inverse participation ratio (IPR) from the calculations on disordered $Ge_1Sb_2Te_4$ of Zhang et al.,[12] the number of atoms taking part in the localized wave functions is around 22 if all vacancies are distributed randomly. This number corresponds to a volume of 0.7 nm^3. With increasing order of the vacancies, the localization length also increases. Hence, the localization length of 1.6 nm is very plausible if the vacancies are assumed to be slightly ordered in the sample investigated here.

At our lowest accessible temperature of 0.35 K, the characteristic hopping length[46] $\overline{r} \approx 0.4 \cdot \xi \cdot \left(\frac{T_M}{T}\right)^{1/4}$ is of the order of 10 nm, i.e., smaller than the grain size which is at least 20 nm.[11] Hence, most hopping events take place within one grain. The hopping length is also smaller than the film thickness, which a posteriori justifies the assumption of 3D transport and hence an exponent of 1/4 in Equation (8).

By using Mott's law, we have assumed the density of states to be constant within the relevant energy range around the Fermi energy. The width of this range is given by[31] $\Delta E = k_B(T^3 \cdot T_M)^{1/4}$, which yields 10 meV at $T = 20$ K. In the parabolic-band model, the density of states varies as $\sqrt{E}$, hence the relative change in the density of states can be estimated as $\frac{\Delta N(E)}{N(E_F)} \approx \frac{1}{2} \cdot \frac{\Delta E}{E_F} = 4\%$. This small number is compatible with the assumption of a constant density of states. Also the OJL model with $\gamma = 60$ meV yields only $\frac{\Delta N(E)}{N(E_F)} \approx 5\%$.

The same analysis is performed for the samples with $\sigma_{300\,K} = 2.9$ S cm^{-1} (sample A) and $\sigma_{300\,K} = 6.6$ S cm^{-1} (sample f) using the same temperature range for the fit. The parameters are listed in **Table 2**. Also for these samples we start to see deviations from Mott VRH below ≈3 K.

Table 2. Parameters derived from the Hopping-law fits. The density of states at the Fermi energy is $N(E_F) = 2.5 \times 10^{21}$ cm^{-3} eV^{-1}. The localization length ξ_M (and ξ_{ES}) is calculated both from the Mott temperature T_M via Equation (9) (and from the Efros–Shklovskii temperature T_{ES} via Equation (14), respectively). The crossover temperature T_x to Efros–Shklosvkii hopping is calculated from ξ_M employing Equation (12) and assuming an $\varepsilon_{st} \approx 98$.

Sample	$\sigma_{0,M}$ [S cm^{-1}]	T_M [K]	ξ_M [nm]	T_x [K]	T_{ES} [K]	ξ_{ES} [nm]
A	19.1	36047	1.3	3.2	100	4.8
F	21.8	19102	1.6	3.9	74	6.4
f	19.1	5692	2.4	5.9	36	13.3

Table 2 also lists the prefactors $\sigma_{0,M}$ in Equation (8) obtained from the fit. According to the derivation of Mott's law (see, e.g., formulae (2.60)–(2.63) in a previous study),[47] the prefactor is given by

$$\sigma_{0,M} = \frac{9}{16} \cdot \sqrt{\frac{3}{2\pi} \cdot e^2 \nu_{ph} \cdot \sqrt{\frac{N(E_F) \cdot \xi}{k_B \cdot T}}} \quad (10)$$

Being employed to calculate the phonon frequency ν_{ph}, this relation may be used as an additional check of consistency. From the numbers in Table 2 and by choosing $T = 12$ K, i.e., in the middle of the fit range, phonon frequencies between 0.4 and 0.6 THz are obtained. This is a reasonable number for an optical phonon involved in hopping transport in this temperature range and further corroborates the validity of Mott's law.

We will now analyze the deviations from Mott's law at the lowest temperatures in our measurements, where the sheet resistance increases even more rapidly than predicted. In the case of strong localization due to disorder, electron–electron interactions become important: The Coulomb interaction of localized charge carriers is expected to cause a soft gap in the electronic density of states,[32] its width being[38]

$$\Delta = e^3 \sqrt{\frac{N(E_F)}{(4\pi\varepsilon_0\varepsilon_{st})^3}} \quad (11)$$

As long as the temperature and hence the typical phonon energy in a hopping event is large compared to this gap, Mott's assumption of a constant density of states is still justified. Only around a crossover temperature T_x of[38]

$$k_B T_x = 0.38 \frac{e^4 \cdot \xi \cdot N(E_F)}{(4\pi\varepsilon_0\varepsilon_{st})^2} \quad (12)$$

and below, the (quadratic) energy dependence of the density of states has to be considered and leads to the Efros–Shklovskii hopping law[48]

$$\sigma = \sigma_{0,ES} \exp\left[-\left(\frac{T_{ES}}{T}\right)^{1/2}\right] \quad (13)$$

with[46]

$$k_B T_{ES} = 2.8 \frac{e^2}{4\pi\varepsilon_0\varepsilon_{st}\xi} \quad (14)$$

The static dielectric constant ε_{st} quadratically enters the denominator in Equation (12). Since crystalline phase-change materials display a large value of ε_{st} of about 98, it seems at first sight surprising that a transition between the two hopping mechanisms should be considered in these materials where Coulomb interactions should be strongly screened. The large Fermi energy and the resulting high density of carriers however overcompensates this effect since it causes the gap to be of the order of 3 meV. Correspondingly, the calculated crossover temperature for the sample with $\sigma_{300\ K}$ = 4.2 S cm^{-1} (sample F) is 4 K, which agrees well with the onset of the low-temperature deviations in Figure 4. In **Figure 5**, we therefore plot the data on a $T^{1/2}$ scale and perform a fit to the portion between 1.6 and 3 K where the data indeed follow a straight line.

The least resistive sample with $\sigma_{300\ K}$ = 6.6 S cm^{-1} (sample f) could even be measured at temperatures down to 0.4 K. In this case, deviations from the straight line are not only observed at higher temperatures, but also below 1 K. These deviations will be discussed further below.

From the resulting fit we obtain a characteristic temperature of 74 K for the sample with $\sigma_{300\ K}$ = 4.2 S cm^{-1} (sample F). This corresponds to a localization length of 6.4 nm as derived from Equation (14).

Especially the numbers derived from the Mott model are considered very trustworthy, because this type of hopping would be expected for strongly localized carriers in a smooth density of states at such temperatures. The only parameter apart from the fit parameter T_M that enters the calculation of ξ is $N(E_F)$. The uncertainty on this quantity is rather small and it only enters to the power of 1/3. However, while the localization lengths derived from the Efros–Shklovskii model are still reasonable, they exceed the former by a factor of 4.

Possible reasons for the deviations shall be discussed here.

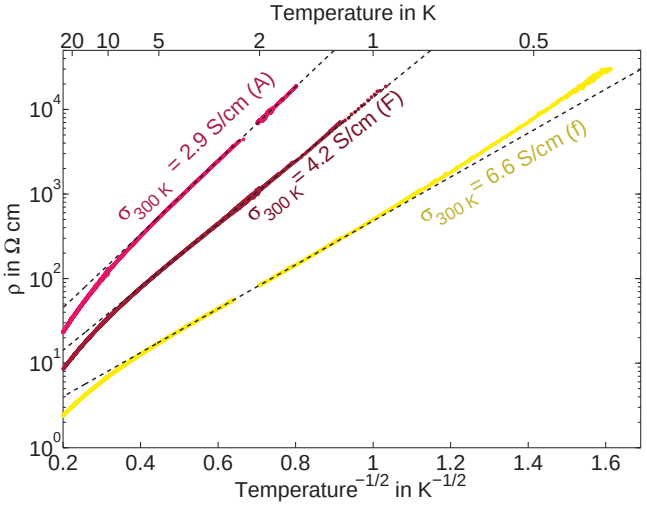

Figure 5. Temperature dependence of the resistance of samples A ($\sigma_{300\ K}$ = 2.9 S cm^{-1}), F ($\sigma_{300\ K}$ = 4.2 S cm^{-1}), and f ($\sigma_{300\ K}$ = 6.6 S cm^{-1}) on an Efros–Shklovskii variable range hopping scale. The dashed lines represent the fits of the data between 1.6 and 3 K to Equation (13) with the fit parameters given in Table 2. Details about the sample properties are given in Table 1.

The calculation of ξ from T_{ES} requires the knowledge of the static dielectric constant ε_{st}. In contrast to $N(E_F)$, this quantity is not well known. Only a lower bound of 98 is predicted from DFT calculations and the correct value might be significantly larger, which would yield smaller localization lengths.

At very low temperatures (<1 K), even the Efros–Shklovskii law seems to fail. While this cannot be validated for the samples with $\sigma_{300\ K}$ = 2.9 and 4.2 S cm^{-1} (samples A and F, respectively) due to their high resistivity, the deviations seen for sample f ($\sigma_{300\ K}$ = 6.6 S cm^{-1}) are significant. A possible interpretation that has been suggested in similar cases is the assumption of a hardening of the Coulomb gap either due to spin interaction or higher-order Coulomb interaction.[17,31,49,50] In such a case, Equation (13) will no longer be obeyed.

Another possible explanation can be found in ref. [51]: The Coulomb gap might be smeared even at such low temperatures. In this case, Equation (13) would only be obeyed at even lower temperatures. While the latter interpretation could also help to resolve the discrepancy between the localization length values in Table 2, the present data do not allow for discrimination between both (and possibly other) explanations.

6. Summary and Conclusions

The low-temperature transport properties of highly disordered films of $Ge_1Sb_2Te_4$ have been studied. It has been confirmed that strong localization renders the highly disordered film insulators, hence a metal–insulator transition takes place. This transition is most likely continuous and, as consistently determined by two different methods, achieved by annealing at a temperature between 200 and 225 °C. The corresponding room-temperature conductivity lies between 25 and 54 S cm^{-1} and the conductivity ratio $r\sigma$ between 0.06 and 0.14. The density of states at the Fermi energy is of the order of $N(E_F) = 2.5 \times 10^{21}\,\mathrm{cm^{-3}\,eV^{-1}}$ throughout all samples. The remarkable observation that electronic states at such a high density are localized due to disorder can be explained by the fact that the highly directional p-orbitals are particularly sensitive to distortions and the presence of vacancies.

Our study of the most insulating samples suggests that variable-range hopping is the dominant conduction mechanism. The localization length of the most insulating sample is of the order of a few nanometers, hence much smaller than the grain size. The observation of a crossover from Mott's law to a different hopping mechanism can be taken as a corroboration of the high density of states at the Fermi energy leading to a significant Coulomb gap.

A sketch of the model of the density of states of an insulating sample is shown in **Figure 6**. Both the Fermi energy and the mobility edge lie relatively deep in the valence band, where we assume the parabolic-band approximation to be valid. Because the states are localized though, a Coulomb gap opens up in the direct vicinity of the Fermi energy. Annealing will shift the mobility edge toward the band edge, eventually causing the transition to the metallic state.

With these findings, the foundation for future investigations of the MIT and its nature, such as a study of the critical behavior, has been laid. We consider $Ge_1Sb_2Te_4$ and related

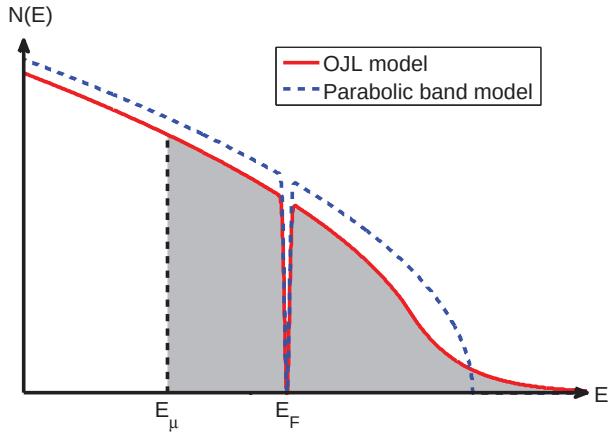

Figure 6. Sketch of the model of the electronic density of states $N(E)$ of the valence band used in this work. E_F marks the Fermi energy and E_μ denotes the mobility edge. Localized states are shaded in gray. Hence, the picture illustrates the situation in an insulating sample. While a Coulomb gap opens up in the close vicinity of E_F, the density of states beyond that gap can be modeled either assuming a parabolic band ($N(E) \propto \sqrt{E}$) or employing the OJL model (Equation (5)). A reduction of disorder by annealing will shift the mobility edge to the right (eventually crossing the Fermi energy) and narrow the exponential tail.

materials a promising playground for studying the MIT in the presence of strong disorder, high charge carrier concentrations, and a large static dielectric constant, i.e., where correlation effects are less pronounced.

Acknowledgements

The authors gratefully acknowledge the support by the Deutsche Forschungsgemeinschaft (SFB 917). Moreover, the research leading to these results had received funding from the European Union Seventh Framework Programme (FP7/2007–2013) under Grant Agreement No. 340698. Furthermore, the authors would like to thank Zvi Ovadyahu, Vladimir Dobrosavljevic, and Vsevolod F. Gantmakher for fruitful discussions.

Received: March 2, 2015
Revised: April 24, 2015
Published online: June 10, 2015

[1] M. Wuttig, N. Yamada, *Nat. Mater.* **2007**, *6*, 824.
[2] W. J. Wang, L. P. Shi, R. Zhao, K. G. Lim, H. K. Lee, T. C. Chong, Y. H. Wu, *Appl. Phys. Lett.* **2008**, *93*, 043121.
[3] G. Bruns, P. Merkelbach, C. Schlockermann, M. Salinga, M. Wuttig, T. D. Happ, J. B. Philipp, M. Kund, *Appl. Phys. Lett.* **2009**, *95*, 043108.
[4] T. Matsunaga, N. Yamada, Y. Kubota, *Acta Crystallogr. Sect. B* **2004**, *60*, 685.
[5] T. Matsunaga, N. Yamada, *Phys. Rev. B* **2004**, *69*, 104111.
[6] M. Wuttig, D. Lüsebrink, D. Wamwangi, W. Wełnic, M. Gilleßen, R. Dronskowski, *Nat. Mater.* **2007**, *6*, 122.
[7] K. Shportko, S. Kremers, M. Woda, D. Lencer, J. Robertson, M. Wuttig, *Nat. Mater.* **2008**, *7*, 653.
[8] D. Lencer, M. Salinga, B. Grabowski, T. Hickel, J. Neugebauer, M. Wuttig, *Nat. Mater.* **2008**, *7*, 972.
[9] T. Zhang, Z. Song, B. Liu, G. Feng, S. Feng, B. Chen, *Thin Solid Films* **2007**, *516*, 42.
[10] E. Prokhorov, G. Trapaga, J. González-Hernández, *J. Appl. Phys.* **2008**, *104*, 103712.
[11] T. Siegrist, P. Jost, H. Volker, M. Woda, P. Merkelbach, C. Schlockermann, M. Wuttig, *Nat. Mater.* **2011**, *10*, 202.
[12] W. Zhang, A. Thiess, P. Zalden, R. Zeller, P. H. Dederichs, J.-Y. Raty, M. Wuttig, S. Blügel, R. Mazzarello, *Nat. Mater.* **2012**, *11*, 952.
[13] P. Nukala, R. Agarwal, X. Qian, M. H. Jang, S. Dhara, K. Kumar, A. T. C. Johnson, J. Li, R. Agarwal, *Nano Lett.* **2014**, *14*, 2201.
[14] N. P. Breznay, H. Volker, A. Palevski, R. Mazzarello, A. Kapitulnik, M. Wuttig, *Phys. Rev. B* **2012**, *86*, 205302.
[15] M. A. Paalanen, T. F. Rosenbaum, G. A. Thomas, R. N. Bhatt, *Phys. Rev. Lett.* **1982**, *48*, 1284.
[16] T. F. Rosenbaum, R. F. Milligan, M. A. Paalanen, G. A. Thomas, R. N. Bhatt, W. Lin, *Phys. Rev. B* **1983**, *27*, 7509.
[17] P. Dai, Y. Zhang, M. P. Sarachik, *Phys. Rev. Lett.* **1991**, *66*, 1914.
[18] A. Möbius, D. Elefant, A. Heinrich, R. Muller, J. Schumann, H. Vinzelberg, G. Zies, *J. Phys. C: Solid State Phys.* **1983**, *16*, 6491.
[19] S. Yoshizumi, T. H. Geballe, M. Kunchur, W. L. McLean, *Phys. Rev. B* **1988**, *37*, 7094.
[20] Q. Guo, S. J. Poon, *Phys. Rev. B* **1996**, *54*, 12793.
[21] C. R. Wang, H. S. Kuan, S. T. Lin, Y. Y. Chen, *J. Phys. Soc. Jpn.* **1998**, *67*, 2383.
[22] T.-I. Su, C.-R. Wang, S.-T. Lin, R. Rosenbaum, *Phys. Rev. B* **2002**, *66*, 054438.
[23] L. J. van der Pauw, *Philips Res. Rep.* **1958**, *13*, 1.
[24] J.-J. Kim, K. Kobayashi, E. Ikenaga, M. Kobata, S. Ueda, T. Matsunaga, K. Kifune, R. Kojima, N. Yamada, *Phys. Rev. B* **2007**, *76*, 115124.
[25] C. Longeaud, J. Luckas, D. Krebs, R. Carius, J. Klomfass, M. Wuttig, *J. Appl. Phys.* **2012**, *112*, 113714.
[26] S. K. O'Leary, S. R. Johnson, P. K. Lim, *J. Appl. Phys.* **1997**, *82*, 3334.
[27] O. Gunnarsson, M. Calandra, J. E. Han, *Rev. Mod. Phys.* **2003**, *75*, 1085.
[28] S. Privitera, C. Garozzo, A. Alberti, L. Perniola, B. De Salvo, *AIP Adv.* **2013**, *3*, 012105.
[29] N. F. Mott, *Adv. Phys.* **1967**, *16*, 49.
[30] E. Abrahams, P. W. Anderson, D. C. Licciardello, T. V. Ramakrishnan, *Phys. Rev. Lett.* **1979**, *42*, 673.
[31] V. F. Gantmakher, *Electrons and Disorder in Solids*, International Series of Monographs on Physics, Oxford University Press, Oxford **2005**.
[32] P. A. Lee, T. V. Ramakrishnan, *Rev. Mod. Phys.* **1985**, *57*, 287.
[33] G. A. Thomas, M. Paalanen, T. F. Rosenbaum, *Phys. Rev. B* **1983**, *27*, 3897.
[34] B. L. Al'tshuler, A. G. Aronov, *Sov. Phys. JETP* **1979**, *50*, 968.
[35] A. Möbius, C. Frenzel, R. Thielsch, R. Rosenbaum, C. J. Adkins, M. Schreiber, H.-D. Bauer, R. Grötzschel, V. Hoffmann, T. Krieg, N. Matz, H. Vinzelberg, M. Witcomb, *Phys. Rev. B* **1999**, *60*, 14209.
[36] A. Möbius, arXiv:1308.1538v1 (cond-mat) **2013**.
[37] N. F. Mott, *Philos. Mag.* **1969**, *19*, 835.
[38] M. Hornung, H. Löhneysen, *Czech. J. Phys.* **1996**, *46*, 2437.
[39] H. Overhof, *Phys. Status Solidi B* **1975**, *67*, 709.
[40] J. M. Marshall, C. Main, *J. Phys.: Condens. Matter* **2008**, *20*, 285210.
[41] I. S. Shlimak, M. J. Lea, P. Fozooni, P. Stefanyi, A. N. Ionov, *Phys. Rev. B* **1993**, *48*, 11796.
[42] H. Liu, A. Pourret, P. Guyot-Sionnest, *ACS Nano* **2010**, *4*, 5211.

[43] R. Rosenbaum, *Phys. Rev. B* **1991**, *44*, 3599.
[44] Z. Ovadyahu, *Phys. Rev. B* **1986**, *33*, 6552.
[45] H. Hosono, N. Kikuchi, N. Ueda, H. Kawazoe, *J. Non-Cryst. Solids* **1996**, *198–200*, 165.
[46] Y. Zhang, O. Dai, M. Levy, M. P. Sarachik, *Phys. Rev. Lett.* **1990**, *64*, 2687.
[47] N. F. Mott, E. A. Davis, *Electronic Processes in Non-Crystalline Solids*, 2nd ed., Clarendon Press, Oxford **1979**.
[48] A. L. Efros, B. I. Shklovskii, *J. Phys. C: Solid State Phys.* **1975**, *8*, L49.
[49] R. W. van der Heijden, G. Chen, A. T. A. M. de Waele, H. M. Gijsman, F. P. B. Tielen, *Solid State Commun.* **1991**, *78*, 5.
[50] I. S. Shlimak, in *Hopping and Related Phenomena*, (Eds: H. Fritzsche, M. Pollak), World Scientific, Singapore **1990**.
[51] I. Shlimak, M. Kaveh, R. Ussyshkin, V. Ginodman, S. D. Baranovskii, P. Thomas, H. Vaupel, R. W. van der Heijden, *Phys. Rev. Lett.* **1995**, *75*, 4764.